

Point Cloud Mapping Using Only Onboard Lidar in GNSS Denied and Dynamic Environments

Misato Yamaji, Seiya Tanaka
Graduate School of Science and Engineering
Doshisha University
Kyotanabe, Kyoto 610-0394 Japan

Masafumi Hashimoto, Kazuhiko Takahashi
Faculty of Science and Engineering
Doshisha University
Kyotanabe, Kyoto 610-0394 Japan
e-mail: {mhashimo, katakaha}@mail.doshisha.ac.jp

Abstract— This paper presents a 3D point cloud mapping in Global Navigation Satellite Systems (GNSS) denied and dynamic outdoor environments using only a scanning multilayer lidar mounted on a vehicle. Distortion in scan data from the lidar is corrected by estimating the vehicle’s pose (3D positions and attitude angles) in a period shorter than the lidar scan period based on Normal Distributions Transform (NDT) scan matching and Extended Kalman Filter (EKF). The corrected scan data are mapped onto an elevation map; static and moving scan data, which are originated from static and moving objects, respectively, in the environments, are classified using the occupancy grid method. Only the static scan data are applied to generate a point cloud map using NDT-based Simultaneous Localization And Mapping (SLAM) and graph-based SLAM. Experimental results in a public road environment show the performance of the proposed method.

Keywords—lidar; point cloud map; distortion correction; NDT SLAM; graph SLAM; GNSS denied environment; dynamic environment.

I. INTRODUCTION

Recently, studies have been conducted on autonomous driving and active safety of vehicles, such as automobiles and personal mobility vehicles, and on autonomous robots for last-mile and first-mile automation. Important technologies in these studies include environmental map generation [1] and map-matching based self-pose estimation by vehicles using the generated maps [2]. A lot of their related studies using cameras, lidars, and radars have been actively conducting [3][4].

In this paper, we focus on map generation with a lidar mounted on a vehicle. When compared with camera (vision) based map generation, lidar based map generation is robust to lighting conditions and require less computational time. Furthermore, lidar based map generation provides mapping accuracy better than radar based map generation due to higher spatial resolution of lidar. From these reasons, we focus on lidar based map generation.

In Intelligent Transportation Systems (ITS) domains, mobile mapping systems are utilized to map generation in wide road environments, such as highways and motorways [5]. We have been studying a method for point cloud mapping (map generation) using only a lidar mounted on a vehicle in narrow road environments, such as at community and scenic roads in urban and mountainous areas [6]. The

generated map could be applied to autonomous driving and navigation of various smart vehicles, such as intelligent wheelchairs, personal mobility vehicles, and delivery robots [7]. The generated maps may also be utilized in various social services, such as disaster prevention and mitigation.

In urban and mountainous environments, the information of Global Navigation Satellite Systems (GNSS) is often disturbed and denied. For map generation in GNSS denied environments, Simultaneous Localization And Mapping (SLAM) using Normal Distributions Transform (NDT) [8] or Iterative Closest Points (ICP) [9] methods have been applied. In their scan matching based SLAM, the accuracy in mapping wide area degrades due to the accumulation error. To reduce the accumulation error, the graph-based SLAM [10] is usually applied. Recently, we presented a map generation method using NDT-based SLAM and graph-based SLAM [6]. A vehicle equipped with a lidar was moved so that loops could be made in road network topology, and several submaps (maps of different small areas) were generated using recursive NDT-based SLAM and graph-based SLAM. Several submaps were also merged using graph-based SLAM. Such approach in submap generation and merging makes it easy to update and maintain maps.

In environments, moving objects, such as automobile, two-wheeled vehicles, and pedestrians, exist. In such dynamic environments, the lidar scan data are therefore classified into two types: scan data originated from moving objects (referred to as moving scan data), and those originated from static objects (static scan data), such as buildings, trees, and traffic poles. For accurate map generation, the moving scan data should be removed, and only the static scan data should be utilized. Several methods for mapping in dynamic environments have been presented [11][12][13]; however, map generation in dynamic environments still represent a significant challenge compared with map generation in static environments. Our map generation method [6] was also applicable in static environments. Apart from map generation, we have been studying moving object detection and tracking in crowded dynamic environments [14][15]. The detection and tracking methods can contribute in accurately generating maps by extracting the static scan data from the lidar data.

Map generation using the onboard lidar is performed by mapping lidar scan data captured in a sensor coordinate frame onto a world coordinate frame using the vehicle’s self-pose (position and attitude angles) information. The

lidar obtains range measurements by scanning lidar beams. Thus, when the vehicle moves, the entire scan data within one scan (lidar beam rotation of 360° in a horizontal plane) cannot be obtained at the same pose of the vehicle. Therefore, if the entire scan data obtained within one scan is mapped onto the world coordinate frame using the vehicle's pose information, distortion arises in environmental maps. To correct this distortion, the vehicle's pose should be determined more frequently than the lidar scan period, i.e., for every lidar measurement in the scan. Many methods for distortion correction have been proposed [16][17][18]. We also presented a distortion correction method using only the lidar information; the NDT scan matching and Extended Kalman Filter (EKF) were applied to estimate the vehicle's pose, and the distortion in the lidar scan data was corrected using the pose estimates [19].

In this paper, to generate a 3D point cloud map in GNSS denied and dynamic environments using only the onboard scanning lidar, we integrate three methods that we previously proposed: distortion correction in the lidar scan data, extraction of the static scan data from the entire lidar scan data, and point cloud mapping based on NDT and graph-based SLAM. The mapping performance is shown through experimental results in public road environments.

The rest of this paper is organized as follows. In Section II, we give the experimental system and overview a map generation method based on NDT-based and graph-based SLAM. In Section III, we explain a correction method of distortion in the lidar scan data, and in Section IV, we describe an extraction method of the static scan data. In Section V, we conduct experiments to verify the proposed method, followed by conclusions in Section VI.

II. EXPERIMENTAL SYSTEM AND SLAM OVERVIEW

In this section, we show our experimental system and briefly describe the scan data mapping using NDT scan matching (NDT-based SLAM) and graph-based SALM.

A. Experimental System

As shown in Fig. 1, our experimental small vehicle is equipped with a scanning 32-layer lidar (Velodyne HDL-32E). The maximum range of the lidar is 70 m, the horizontal viewing angle is 360° with a resolution of 0.16° , and the vertical viewing angle is 41.34° with a resolution of



Figure 1. Overview of the experimental vehicle.

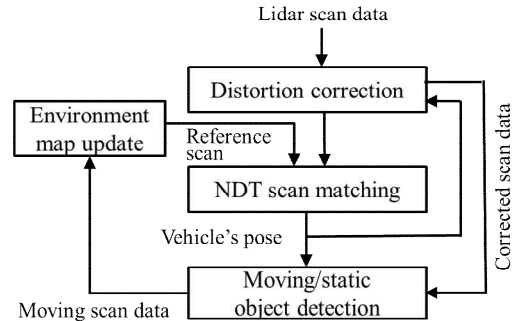


Figure 2. Overview of NDT-based SLAM.

1.33° . The lidar provides 384 measurements (the object's 3D position and reflection intensity) every 0.55 ms (at 2° horizontal angle increments). The period for the lidar beam to complete one rotation (360°) in the horizontal direction is 100 ms, and 70,000 measurements are then obtained in one rotation.

In this paper, one rotation of the lidar beam in the horizontal direction (360°) is referred to as one scan, and the data obtained from this scan is referred to as scan data. Moreover, the lidar scan period (100 ms) is denoted as τ and scan data observation period (0.55 ms) as $\Delta\tau$.

B. NDT-based SLAM

The process for NDT-based SLAM is shown in Fig. 2. To be clear, the NDT scan matching [8] is described in this subsection. Distortion correction method is detailed in the following section.

First of all, the scan data related to road surfaces are removed, and the scan data related to objects are mapped onto a 3D grid map (a voxel map) represented in the vehicle's coordinate frame, Σ_b . A voxel grid filter is applied to downsize the scan data. The voxel used for the voxel grid filter is a tetrahedron with a side length of 0.2 m.

In the world coordinate frame, Σ_w , a voxel map with a voxel size of 1 m is used for NDT scan matching. For the i -th ($i = 1, 2, \dots, n$) measurement in the scan data, we define the position vector in Σ_b as \mathbf{p}_{bi} and that in Σ_w as \mathbf{p}_i . Thus, the following relation is given by the homogeneous form:

$$\begin{pmatrix} \mathbf{p}_i \\ 1 \end{pmatrix} = \mathbf{T}(X) \begin{pmatrix} \mathbf{p}_{bi} \\ 1 \end{pmatrix} \quad (1)$$

where $X = (x, y, z, \phi, \theta, \psi)^T$ is the vehicle's pose. $(x, y, z)^T$ and $(\phi, \theta, \psi)^T$ are the 3D position and attitude angle (roll, pitch, and yaw angles) of the vehicle, respectively, in Σ_w . $\mathbf{T}(X)$ is the following homogeneous transformation matrix:

$$\mathbf{T}(X) = \begin{pmatrix} \cos \theta \cos \psi & \sin \phi \sin \theta \cos \psi - \cos \phi \sin \psi & \cos \phi \sin \theta \cos \psi + \sin \phi \sin \psi & x \\ \cos \theta \sin \psi & \sin \phi \sin \theta \sin \psi + \cos \phi \cos \psi & \cos \phi \sin \theta \sin \psi - \sin \phi \cos \psi & y \\ -\sin \theta & \sin \phi \cos \theta & \cos \phi \cos \theta & z \\ 0 & 0 & 0 & 1 \end{pmatrix}$$

The scan data obtained at the current time $t\tau$ ($t = 0, 1, 2, \dots$), $\mathbf{p}_b^{(t)} = \{\mathbf{p}_{b1}^{(t)}, \mathbf{p}_{b2}^{(t)}, \dots\}$, are referred to as the new input scan, and the scan data obtained in the previous time before $(t-1)\tau$, $\mathbf{P} = \{\mathbf{P}^{(0)}, \mathbf{P}^{(1)}, \dots, \mathbf{P}^{(t-1)}\}$, are referred to as the reference scan (environmental map).

NDT scan matching conducts a normal distribution transformation for the reference scan data in each grid on a voxel map. It calculates the average value and covariance of the lidar measurement positions. By matching the new input scan at $t\tau$ with the reference scan data obtained prior to $(t-1)\tau$, the vehicle's pose, $\mathbf{X}^{(t)}$, at $t\tau$ is determined. The vehicle's pose is used for conducting a coordinate transform with (1), and the new input scan can then be mapped to Σ_w , and the reference scan is updated.

C. Graph-based SLAM

To reduce the accumulation error of the map generated by NDT-based SLAM, we apply the graph-based SLAM [20]. The vehicle's poses obtained by NDT-based SLAM are mapped onto a factor graph. To detect the loop (revisit area), we first obtain the candidates of the revisit areas using the information on self poses of the vehicle. Thereafter, the loop probability indicator (LPI) [21] and matching distance indicator (MDI) are calculated using the lidar scan data captured during the initial visit and revisit of the vehicle. A higher degree of similarity between the lidar scan data of the initial visit and revisit of the vehicle will lead to a larger LPI and a smaller MDI. Thus, we detect the loop using the LPI and MDI values.

When the loop is detected, the vehicle's pose is calculated at the revisit area relative to that at the first-visit area based on NDT scan matching. The relative poses of the vehicle are inputted to the factor graph as loop constraints. We then minimize the objective function of (2) so that the accuracy in the map generated by the NDT-based SLAM can be improved [21]:

$$F(\boldsymbol{\chi}) = \sum_{i,j} (\Delta \mathbf{X}_{ij} - \Delta \hat{\mathbf{X}}_{ij})^T \boldsymbol{\Omega}_{ij} (\Delta \mathbf{X}_{ij} - \Delta \hat{\mathbf{X}}_{ij}) \quad (2)$$

where $\boldsymbol{\chi} = (\mathbf{X}_1^T, \mathbf{X}_2^T, \dots, \mathbf{X}_i^T)^T$. \mathbf{X}_i is the vehicle's pose at the $i\tau$. $\Delta \mathbf{X}_{ij}$ is the pose of the vehicle at the $j\tau$ relative to that at the $i\tau$, which is calculated from NDT scan matching. $\Delta \hat{\mathbf{X}}_{ij}$ is the estimate of the relative pose. $\boldsymbol{\Omega}_{ij}$ is the information matrix.

III. DISTORTION CORRECTION OF LIDAR SCAN DATA

In this section, we describe a motion model of the vehicle for EKF and EKF-based correction method of distortion in lidar scan data.

A. Motion Model

As shown in Fig. 3, the vehicle's linear velocity in Σ_b is defined as V_b (the velocity in the x_b -axis direction), and the angular velocities about the x_b -, y_b -, and z_b - axes are defined as $\dot{\phi}_b$, $\dot{\theta}_b$, and $\dot{\psi}_b$, respectively. If the vehicle is assumed to move at nearly constant linear and angular velocities, the following motion model can be derived:

$$\begin{pmatrix} x^{(t+1)} \\ y^{(t+1)} \\ z^{(t+1)} \\ \phi^{(t+1)} \\ \theta^{(t+1)} \\ \psi^{(t+1)} \\ V_b^{(t+1)} \\ \dot{\phi}_b^{(t+1)} \\ \dot{\theta}_b^{(t+1)} \\ \dot{\psi}_b^{(t+1)} \end{pmatrix} = \begin{pmatrix} x^{(t)} + a_1^{(t)} \cos \theta^{(t)} \cos \psi^{(t)} \\ y^{(t)} + a_1^{(t)} \cos \theta^{(t)} \sin \psi^{(t)} \\ z^{(t)} - a_1^{(t)} \sin \theta^{(t)} \\ \phi^{(t)} + a_2^{(t)} + \{a_3^{(t)} \sin \phi^{(t)} + a_4^{(t)} \cos \phi^{(t)}\} \cdot \tan \theta^{(t)} \\ \theta^{(t)} + \{a_3^{(t)} \cos \phi^{(t)} - a_4^{(t)} \sin \phi^{(t)}\} \\ \psi^{(t)} + \{a_3^{(t)} \sin \phi^{(t)} + a_4^{(t)} \cos \phi^{(t)}\} \\ \frac{1}{\cos \theta^{(t)}} \\ V_b^{(t)} + \tau w_{V_b} \\ \dot{\phi}_b^{(t)} + \tau w_{\dot{\phi}_b} \\ \dot{\theta}_b^{(t)} + \tau w_{\dot{\theta}_b} \\ \dot{\psi}_b^{(t)} + \tau w_{\dot{\psi}_b} \end{pmatrix} \quad (3)$$

where t and $t+1$ are time steps. $a_1 = V_b \tau + \tau^2 w_{V_b} / 2$, $a_2 = \dot{\phi}_b \tau + \tau^2 w_{\dot{\phi}_b} / 2$, $a_3 = \dot{\theta}_b \tau + \tau^2 w_{\dot{\theta}_b} / 2$ and $a_4 = \dot{\psi}_b \tau + \tau^2 w_{\dot{\psi}_b} / 2$. w_{V_b} , $w_{\dot{\phi}_b}$, $w_{\dot{\theta}_b}$, and $w_{\dot{\psi}_b}$ are the acceleration disturbances.

Equation (3) is expressed in the vector form as follows:

$$\boldsymbol{\xi}^{(t+1)} = \mathbf{f}[\boldsymbol{\xi}^{(t)}, \mathbf{w}, \tau] \quad (4)$$

where $\boldsymbol{\xi} = (x, y, z, \phi, \theta, \psi, V_b, \dot{\phi}_b, \dot{\theta}_b, \dot{\psi}_b)^T$ and $\mathbf{w} = (w_{V_b}, w_{\dot{\phi}_b}, w_{\dot{\theta}_b}, w_{\dot{\psi}_b})^T$.

We define the vehicle's pose obtained at $t\tau$ using NDT scan matching as $\mathbf{z}_{NDT}^{(t)} \equiv \mathbf{X}^{(t)}$. The measurement equation is then

$$\mathbf{z}_{NDT}^{(t)} = \mathbf{H} \boldsymbol{\xi}^{(t)} + \Delta \mathbf{z}_{NDT}^{(t)} \quad (5)$$

where $\Delta \mathbf{z}_{NDT}$ is the measurement noise, and \mathbf{H} is the measurement matrix.

B. EKF-based Distortion Correction

The flow of distortion correction of the lidar scan data is shown in Fig. 4. The lidar scan period (τ) is 100 ms, and the scan data observation period ($\Delta \tau$) is 0.55 ms. When the scan data are mapped onto Σ_w using the vehicle's pose

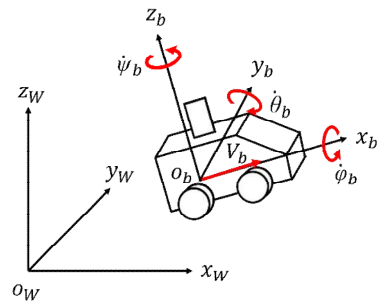


Figure 3. Notation related to vehicle motion.

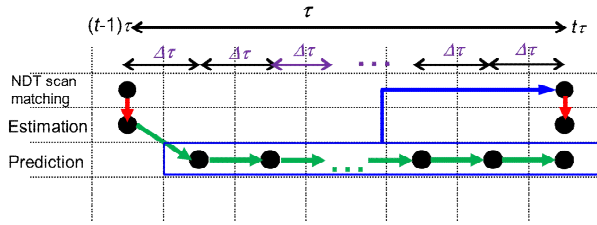


Figure 4. The flow of distortion correction.

calculated every lidar scan period, the distortion arises in environmental maps. We therefore correct the distortion in the lidar scan data by estimating the vehicle's pose using EKF every scan data observation period.

The state estimate and its error covariance obtained at $(t-1)\tau$ using EKF are denoted as $\hat{\xi}_{(t-1/t-1)}$ and $\Gamma_{(t-1/t-1)}$, respectively. From these estimates, EKF gives the state prediction, $\hat{\xi}_{(t-1,t/t-1)}$, and its error covariance, $\Gamma_{(t-1,t/t-1)}$, at $(t-1)\tau + \Delta\tau$ as follows:

$$\left. \begin{aligned} \hat{\xi}_{(t-1,t/t-1)} &= \mathbf{f}[\hat{\xi}_{(t-1/t-1)}, 0, \Delta\tau] \\ \Gamma_{(t-1,t/t-1)} &= \mathbf{F}_{(t-1/t-1)}\Gamma_{(t-1/t-1)}\mathbf{F}_{(t-1/t-1)}^T \\ &\quad + \mathbf{G}_{(t-1/t-1)}\mathbf{Q}\mathbf{G}_{(t-1/t-1)}^T \end{aligned} \right\} \quad (6)$$

where $\mathbf{F} = \partial\mathbf{f}/\partial\hat{\xi}$, $\mathbf{G} = \partial\mathbf{f}/\partial\mathbf{w}$, and \mathbf{Q} is the covariance matrix of the plant noise, \mathbf{w} .

By a similar calculation, the state prediction, $\hat{\xi}_{(t-1,j/t-1)}$, and its error covariance, $\Gamma_{(t-1,j/t-1)}$, at $(t-1)\tau + j\Delta\tau$ (where $j = 1, 2, \dots, 180$) can be obtained by

$$\left. \begin{aligned} \hat{\xi}_{(t-1,j/t-1)} &= \mathbf{f}[\hat{\xi}_{(t-1,j-1/t-1)}, 0, \Delta\tau] \\ \Gamma_{(t-1,j/t-1)} &= \mathbf{F}_{(t-1,j-1/t-1)}\Gamma_{(t-1,j-1/t-1)}\mathbf{F}_{(t-1,j-1/t-1)}^T \\ &\quad + \mathbf{G}_{(t-1,j-1/t-1)}\mathbf{Q}\mathbf{G}_{(t-1,j-1/t-1)}^T \end{aligned} \right\} \quad (7)$$

In the state prediction $\hat{\xi}_{(t-1,j/t-1)}$, we denote the elements related to the vehicle's pose, $(x, y, z, \theta, \phi, \psi)$, as $\hat{\mathbf{X}}_{(t-1,j/t-1)}$. Using (1) and the pose prediction, the scan data, $\mathbf{p}_{bi}^{(t-1,j)}$, in Σ_b obtained at $(t-1)\tau + j\Delta\tau$ can be transformed to $\mathbf{p}_i^{(t-1,j/t-1)}$ in Σ_w as follows:

$$\begin{pmatrix} \mathbf{p}_i^{(t-1,j/t-1)} \\ 1 \end{pmatrix} = \mathbf{T}(\hat{\mathbf{X}}_{(t-1,j/t-1)}) \begin{pmatrix} \mathbf{p}_{bi}^{(t-1,j)} \\ 1 \end{pmatrix} \quad (8)$$

Because the lidar scan period (τ) is 100 ms, and the scan data observation period ($\Delta\tau$) is 0.55 ms, the time $t\tau$ is almost equal to $(t-1)\tau + 180\Delta\tau$. Using the pose prediction, $\hat{\mathbf{X}}_{(t-1,180/t-1)}$ at $t\tau$, the scan data, $\mathbf{p}_i^{(t-1,j/t-1)}$, at $(t-1)\tau + j\Delta\tau$ in Σ_w is transformed into the scan data, $\mathbf{p}_{bi}^{*(t)}$, at $t\tau$ in Σ_b as follows:

$$\begin{pmatrix} \mathbf{p}_{bi}^{*(t)} \\ 1 \end{pmatrix} = \mathbf{T}(\hat{\mathbf{X}}_{(t-1,180/t-1)})^{-1} \begin{pmatrix} \mathbf{p}_i^{(t-1,j/t-1)} \\ 1 \end{pmatrix} \quad (9)$$

Using the corrected scan data, $\mathbf{p}_b^{*(t)} = \{\mathbf{p}_{b1}^{*(t)}, \mathbf{p}_{b2}^{*(t)}, \dots\}$, within one scan (lidar beam rotation of 360° in a horizontal plane), as the new input scan, NDT scan matching can accurately calculate the vehicle's pose, $\mathbf{z}_{NDT}^{(t)}$, at $t\tau$. Based on (4) and (5), EKF then gives the state estimate, $\hat{\xi}_{(t/t)}$, and its error covariance, $\Gamma_{(t/t)}$, at $t\tau$ by

$$\left. \begin{aligned} \hat{\xi}_{(t/t)} &= \hat{\xi}_{(t-1,180/t-1)} + \mathbf{K}_{(t)}\{\mathbf{z}_{NDT}^{(t)} - \mathbf{H}\hat{\xi}_{(t-1,180/t-1)}\} \\ \Gamma_{(t/t)} &= \Gamma_{(t-1,180/t-1)} - \mathbf{K}_{(t)}\mathbf{H}\Gamma_{(t-1,180/t-1)} \end{aligned} \right\} \quad (10)$$

where $\hat{\xi}_{(t-1,180/t-1)}$ and $\Gamma_{(t-1,180/t-1)}$ are the state prediction and its error covariance at $t\tau (= (t-1)\tau + 180\Delta\tau)$, respectively. $\mathbf{K}_{(t)} = \Gamma_{(t-1,180/t-1)}\mathbf{H}^T\mathbf{S}^{-1}_{(t)}$ and $\mathbf{S}_{(t)} = \mathbf{H}\Gamma_{(t-1,180/t-1)}\mathbf{H}^T + \mathbf{R}$. \mathbf{R} is the covariance matrix of $\Delta\mathbf{z}_{NDT}$.

The corrected scan data $\mathbf{p}_b^{*(t)}$ are mapped onto Σ_w using the pose estimate calculated by (10), and the distortion in environmental maps can then be removed.

IV. EXTRACTION OF STATIC SCAN DATA

In dynamic environments wherein moving objects, such as cars, two-wheeled vehicles, and pedestrians, exist, the lidar scan data related to moving objects (referred to as moving scan data) should be removed from the entire scan data, and only the scan data related to static objects (static scan data), such as buildings and trees, should be utilized in map generation.

To extract the static scan data, first, we classify the lidar scan data into two types: scan data that are originated from road surfaces (referred to as road surface scan data) and scan data that are originated from objects (referred to as object scan data) based on a rule-based method. The object scan data are mapped onto an elevation map represented in Σ_w . In this study, the cell of the elevation map is a square with a side length of 0.3 m.

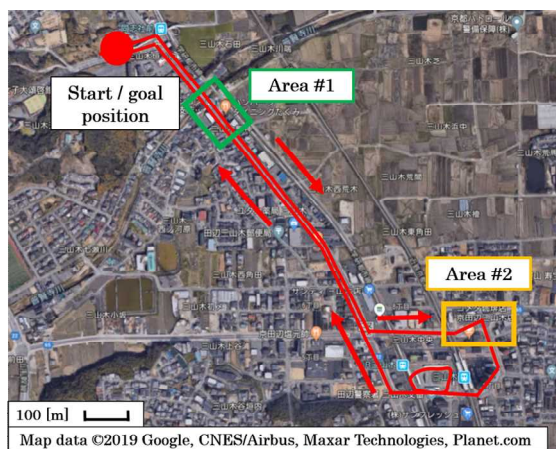
A cell in which scan data exist is referred to as an occupied cell. For the moving scan data, the time to occupy the same cell is short, whereas for the static scan data, the time is long. Therefore, using the occupancy grid method based on the cell occupancy time [14][15], we identify two types of cells: moving and static cells, which are occupied by the moving and static scan data, respectively. Since the scan data related to an object usually occupy more than one cell, adjacent occupied cells are clustered. Then, the scan data in clustered static cells are applied to map generation.

When moving objects pause, the occupancy grid-based method mentioned above often misidentifies their scan data as the static scan data. To address this problem, the road surface scan data are mapped onto the elevation map, and the cells in which the road surface scan data are occupied for a while are determined as the road surface cells. If the object scan data exist on the road surface cells, we always determine the object scan data as the moving scan data and remove the moving scan data from the entire scan data.

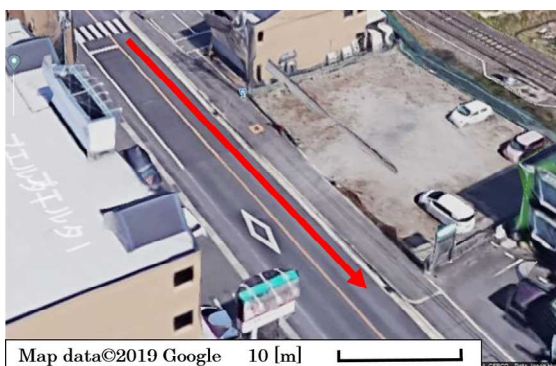
V. EXPERIMENTAL RESULTS

Although as mentioned in Section I, our study focuses on map generation in narrow road environments, such as community roads and scenic roads in urban and mountainous areas, we conducted experiments of map generation in highly traffic road environments (Fig. 5(a)) to discuss the performance of our method in dynamic environments.

The traveled distance of the vehicle was about 2903 m, and the maximum speed of the vehicle was 40 km/h. In the urban road environment, there were 114 cars, 26 two-



(a) Moved path (red line) of the vehicle (top view).



(b) Photo of area #1 (bird-eye view). Red line indicates moved path of the vehicle



(c) Photo of area #2 (bird-eye view). Red line indicates moved path of the vehicle

Figure 5. Experimental environment.

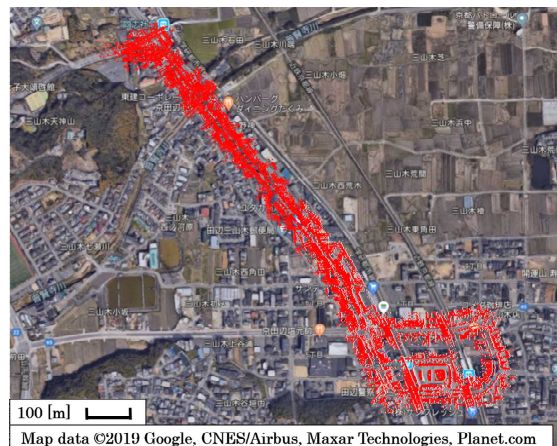
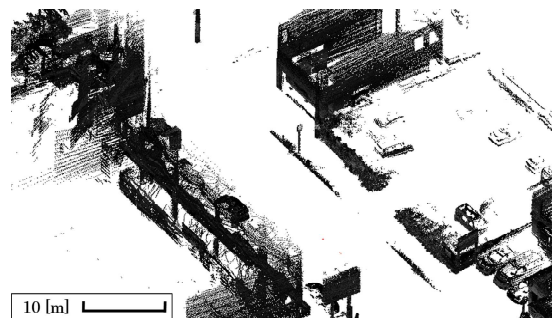
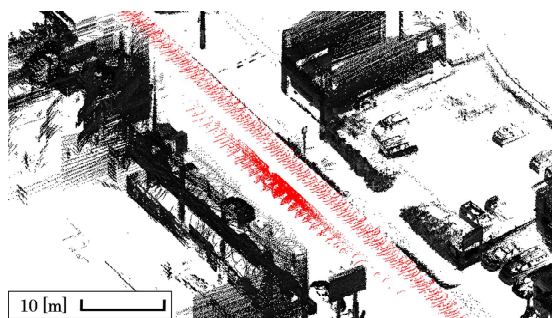


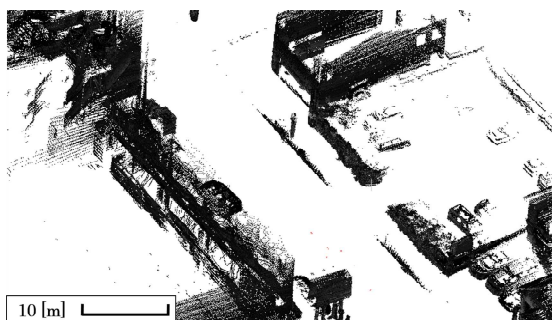
Figure 6. Point cloud map (top view)



(a) Case 1



(b) Case 2



(c) Case 3

Figure 7. Mapping result of area #1 (bird-eye view). Black and red dots indicate the static and moving scan data, respectively.

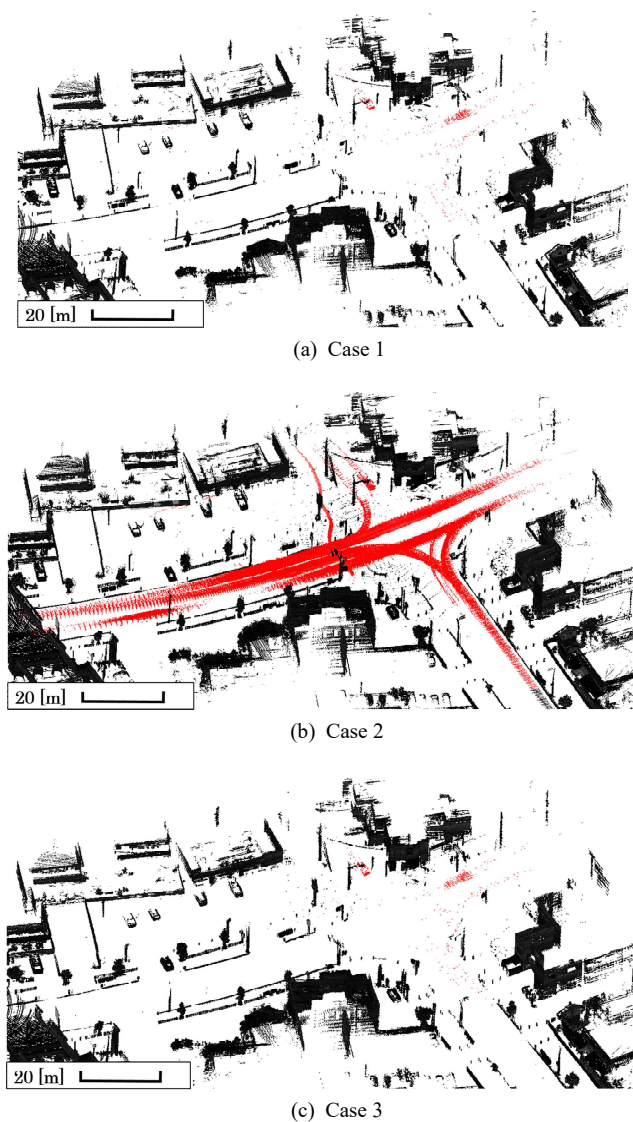


Figure 8. Mapping result of area #2 (bird-eye view). Black and red dots indicate the static and moving scan data, respectively.

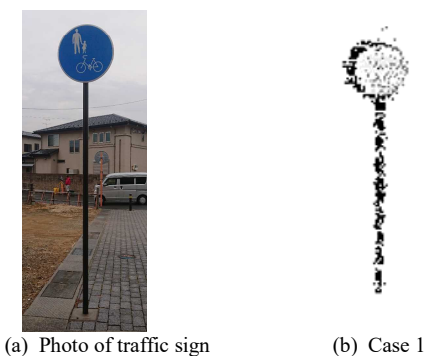


Figure 9. Mapping result of a tree in area #2.

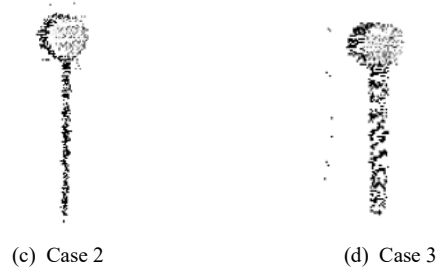


Figure 9. Continued.

TABLE I. DEVIATION BETWEEN START AND GOAL POSITIONS OF THE VEHICLE

True	NDT-based SLAM			NDT and graph-based SLAM
	Case 1	Case 2	Case 3	
2.88 [m]	22.41 [m]	18.48 [m]	132.16 [m]	4.98 [m]

wheeled vehicles, and 37 pedestrians.

Figure 6 shows the mapping result using the NDT-based SLAM in conjunction with the methods of distortion correction of the lidar scan data and extraction of the static scan data. To evaluate the mapping performance using the NDT-based SLAM in detail, Figs. 7 and 8 show the enlarged map of area #1 (Fig. 5 (b)) and #2 (Fig. 5 (c)), respectively. Figure 9 also shows the mapping result of a traffic sign in area #2. For comparison purpose, the maps were generated in the following three cases:

Case 1: Mapping by the proposed method; NDT-based SLAM with the methods of correcting distortion in the lidar scan data and extracting the static scan data,

Case 2: NDT-based SLAM with the distortion correction method and without the method of static scan data extraction, and

Case 3: NDT-based SLAM without the distortion correction method and with the method of static scan data extraction.

In Figs. 7 and 8, case 1 (proposed method) and 3 more significantly remove the track of moving objects than case 2. In Fig. 9, the mapping results by case 1 and 2 are more crispness than the result by case 3. It is concluded from these figures that the proposed method provides better mapping result than case 2 and 3.

Table I shows the positioning performance of the vehicle by SLAM; deviation between the start and goal positions of the vehicle. The true deviation is calculated from the position information using the onboard Real Time Kinematic-Global Positioning Systems (RTK-GPS) unit. It is clear from the table that distortion correction of the lidar scan data provides better mapping accuracy in NDT-based SLAM. In addition, it is clear that graph-based SLAM further improves the mapping accuracy.

VI. CONCLUSION

This paper presented lidar based map generation in GNSS denied and dynamic outdoor environments using only the onboard scanning lidar. The 3D point cloud mapping was performed by integrating three algorithms that we previously proposed: distortion correction in the lidar scan data, extraction of the static scan data (removal of the moving scan data) from the entire lidar scan data, and NDT-based and graph-based SLAM. The performance of the map generation was shown through experimental results in urban road environments.

We are currently improving performance of removal of moving scan data. We are also evaluating the proposed method in various environments, including large-scale residential environments.

ACKNOWLEDGMENT

This study was partially supported by the KAKENHI Grant #18K04062, the Japan Society for the Promotion of Science (JSPS).

REFERENCES

- [1] C. Cadena, et al., "Past, Present, and Future of Simultaneous Localization and Mapping: Toward the Robust-Perception Age," *IEEE Trans. on Robotics*, vol. 32, no. 6, pp. 1309–1332, 2016.
- [2] L. Wang, Y. Zhang, and J. Wang, "Map-Based Localization Method for Autonomous Vehicles Using 3D-LIDAR," *IFAC-Papers OnLine*, vol. 50, issue 1, pp. 276-281, 2017.
- [3] B. Huang, J. Zhao, and J. Liu, "A Survey of Simultaneous Localization and Mapping," eprint arXiv:1909.05214, 2019.
- [4] S. Kuutti, et al., "A Survey of the State-of-the-Art Localization Techniques and Their Potentials for Autonomous Vehicle Applications," *IEEE Internet of Things Journal*, vol.5, pp.829–846, 2018.
- [5] H. G. Seif and X. Hu, "Autonomous Driving in the iCity—HD Maps as a Key Challenge of the Automotive Industry," *Engineering*, vol. 2, pp.159–162, 2016.
- [6] K. Morita, M. Hashimoto, and K. Takahashi, "Point-Cloud Mapping and Merging using Mobile Laser Scanner," *Proc. of the third IEEE Int. Conf. on Robotic Computing (IRC 2019)*, pp.417–418, 2019.
- [7] D. Schwesinger, A. Shariati, C. Montella, and J. Spletzer, "A Smart Wheelchair Ecosystem for Autonomous Navigation in Urban Environments," *Autonomous Robot*, vol. 41, pp. 519–538, 2017.
- [8] P. Biber and W. Strasser, "The Normal Distributions Transform: A New Approach to Laser Scan Matching," *Proc. of IEEE/RSJ Int. Conf. on Intelligent Robots and Systems (IROS 2003)*, pp. 2743–2748, 2003.
- [9] P. J. Besl and N. D. McKay, "A Method of Registration of 3-D Shapes," *IEEE Trans. on Pattern Analysis and Machine Intelligence*, vol. 14, no. 2, pp. 239–256, 1992.
- [10] G. Grisetti, R. Kummerle, C. Stachniss, and W. Burgard, "A Tutorial on Graph-based SLAM," *IEEE Intelligent Transportation Systems Magazine*, pp. 31–43, 2010.
- [11] G. Bresson, Z. Alsayed, L. Yu, and S. Glaser, "Simultaneous Localization and Mapping: A Survey of Current Trends in Autonomous Driving," *IEEE Trans. on Intelligent Vehicles*, vol. 2, pp.194–220, 2017.
- [12] J. P. Saarinen, H. Andreasson, T. Stoyanov, and A. J. Lilienthal, "3D Normal Distributions Transform Occupancy Maps: An Efficient Representation for Mapping in Dynamic Environments," *Int. J. of Robotics Research*, vol.32, no.14, pp.1627–1644, 2013.
- [13] X. Ding, Y. Wang, H. Yin, L. Tang, and R. Xiong, "Multi-session Map Construction in Outdoor Dynamic Environment," *Proc. of the 2018 IEEE Int. Conf. on Real-time Computing and Robotics (IRC2018)*, pp. 384–389, 2018.
- [14] S. Sato, M. Hashimoto, M. Takita, K. Takagi, and T. Ogawa, "Multilayer Lidar-Based Pedestrian Tracking in Urban Environments," *Proc. of IEEE Intelligent Vehicles Symp. (IV2010)*, pp. 849–854, 2010.
- [15] S. Kanaki, et al., "Cooperative Moving-Object Tracking with Multiple Mobile Sensor Nodes -Size and Posture Estimation of Moving Objects using In-vehicle Multilayer Laser Scanner-," *Proc. of 2016 IEEE Int. Conf. on Industrial Technology (ICIT 2016)*, pp. 59–64, 2016.
- [16] S. Hong, H. Ko, and J. Kim, "VICP: Velocity Updating Iterative Closest Point Algorithm," *Proc. of 2010 IEEE Int. Conf. on Robotics and Automation (ICRA 2010)*, pp. 1893–1898, 2010.
- [17] F. Moosmann and C. Stiller, "Velodyne SLAM," *Proc. of IEEE Intelligent Vehicles Symp. (IV2011)*, pp. 393–398, 2011.
- [18] J. Zhang and A. Singh, "LOAM: Lidar Odometry and Mapping in Real-time," *Proc. of Robotics: Science and Systems*, 2014.
- [19] K. Inui, M. Morikawa, M. Hashimoto, and K. Takahashi, "Distortion Correction of Laser Scan Data from In-vehicle Laser Scanner based on Kalman Filter and NDT Scan Matching," *Proc. of the 14th Int. Conf. on Informatics in Control, Automation and Robotics (ICINCO)*, pp. 329–334, 2017.
- [20] R. Kümmerle, G. Grisetti, H. Strasdat, K. Konolige, and W. Burgard, "G2o: A General Framework for Graph Optimization," *Proc. of 2011 IEEE Int. Conf. on Robotics and Automation*, pp. 3607–3613, 2011.
- [21] F. Martin, R. Triebel, L. Moreno, and R. Siegwart, "Two Different Tools for Three-dimensional Mapping: DE-based Scan Matching and Feature-based Loop Detection," *Robotica*, vol. 32, pp. 19–41, 2017.